JSEE Vol. 22, No. 3, 2020 DOI:10.48303/jsee.2020.254238

Research Paper

Structural Health Monitoring of Bridges Based on Vision Method Using Shiny Targets

Mohammad Reza Nikomanesh[1], Hossein Emamjomeh[2], and Mohammad Ali Goudarzi[3*]

1. Ph.D. Candidate, International Institute of Earthquake Engineering and Seismology (IIEES), Tehran, Iran
2. Ph.D. Alumni, International Institute of Earthquake Engineering and Seismology (IIEES), Tehran, Iran
3. Associate Professor, Structural Engineering Research Center, International Institute of Earthquake Engineering and Seismology (IIEES), Tehran, Iran,
*Corresponding Author; email: m.a.goodarzi@iiees.ac.ir

Received: 16/07/2022
Revised: 31/07/2022
Accepted: 24/08/2022

ABSTRACT

In this study, a displacement monitoring technique using an economy camera based on the vision-based method is proposed and developed. The structural displacement can be extracted by utilizing an ordinary shiny device that is attached to one of the elements of the structure and monitoring its motion by an economy video camera. In the proposed vision-based methodology, shiny targets such as LED targets are used to obtain more high-quality images with higher contrast that lead to getting better displacement recording from the captured video. First, a LED centroid recognition and scaling method are described to obtain the time history of structural movements due to the ambient vibration. Next, the natural frequencies of the structure can be determined by utilizing different classical system identification methods in the frequency domain and time domain, like the Peak Picking method and the SSI method. Finally, as a case study, the proposed methodology used for the Tabiat bridge in Tehran, which is a three-dimensional steel truss bridge for pedestrians over a heavy traffic highway, the results are compared with those obtained from the high-accurate and expensive wireless seismic sensors. The results show that although the vision-based proposed technique is a fast and low-cost method, it can investigate the dynamic characteristics of the structure with reasonable precision.

Keywords:
Vision-based Method; Structural Health Monitoring; Structural Dynamic Characteristics; Image Processing; Tabiat Bridge

1. Introduction

Civil infrastructure such as large-scale buildings, bridges, and lifeline systems are exposed to various external loads throughout their service time. Vibration caused by earthquakes, wind, or human-made excitation initiates structural damage during their lifetime and subsequently, triggers catastrophic failure. Structural Health Monitoring (SHM) is an urgent and powerful diagnostic tool for damage detection and catastrophe mitigation of mentioned structures. The SHM includes these parts: data acquisition, system identification, condition evaluation, and maintenance. The SHM methods use responses such as vibration and local responses such as strains or a combination of both to assess the structure during in-service conditions or extreme climatic events. Most of these techniques are primarily responsible for acceleration measurements that require the installation of either contact or non-contact sensors to collect wealthy quality data.

To face the problems of contact sensors, there has been considerable development of noncontact sensors over the last three decades. Sensors based

on GPS [1-3] provided a comfortable operation remote non-intrusive approach to the SHM. However, the GPS can be sensitive to electromagnetic noise, environmental interference, and weather conditions. Unlike GPS, noncontact laser vibrometers and radar interferometry [4-7] provide high-quality measurements. Nevertheless, these devices are expensive and have restrictions on outdoor conditions. The above challenges of noncontact sensors are eliminated with the recent development of other types of vision-based sensors that are integrated with visual and mobile monitoring systems. Such alternate smart sensing techniques include digital and high-speed cameras, UAVs, and smartphone sensors. These sensors are easier and user-friendly, allow simple installation, and offer data recording that is more reliable with high-resolution information of the structures while they are highly cost-effective.

Moreover, there is a significant growth in economy vision-based sensing technology and image pro-cessing. High-speed cameras and consumer-grade DSLR cameras have been used for data acquisition. Cameras are determined by frames per second (fps), pixels, bandwidth, and image consolidation. The current camera-based methods are various in character and range from digital image correlation (DIC) to motion magnification (MM). The vision-based SHM methods consist of these steps: camera calibration, image processing, motion measurement, and damage detection. Still, the DIC has become so general, that a low level of motion related to high-frequency excitation makes it a challenge. The motion magnification method is developed to magnify the small movements of the structure. The combination of the DIC and MM improve system identification to identify structure dynamic characteristic and displacement measurement at low displacements under high-frequency excitation [8]. Trebuna and Hagara [9] proposed a modification of a high-speed correlation method to estimate the dynamic characteristics of steel plates. Feng et al. [10] developed a new vision-based sensor to measure dynamic displacements from video images without using a target-marker panel. The recommended sensor included low-cost charge coupled video cameras with telescopic lenses for real-time extraction of displacements of video images recorded at a rate of 150 fps. Orientation code matching (OCM) algorithm36 was used for image processing that abled tracking of existing structure remotely. Walker [11] studied the condition evaluation of timber structures using virtual vision sensors. This study concentrated on the specification of natural frequencies by monitoring the severity value of each pixel coordinate over the course of a few seconds of a video of vibration and then using a Fast Fourier Transform (FFT) to obtain the frequencies. The resulting natural frequencies of the bridge were extracted to be analogous to the accelerometers. The further advantages of virtual visual sensors include the capability to use multiple data points and not be bounded up to a single plane of motion. The easily existing consumer-grade cameras have shown an encouraging future for their use in Structural Health Monitoring. Fukuda et al. [12] developed a vision-based low-cost system to monitor large-size infrastructure using a digital camcorder and computer with preinstalled image-processing software. The recommended technique used dis-placement parameters based on a target and motion of point for dynamic analysis of the structures and was further upgraded by containing time simultaneously measurement. In Feng and Feng [13] the multipoint displacement for a three-story frame structure was evaluated using two advanced template matching techniques: the unsampled cross-correlation and the OCM. The extracted results from a camera, laser point displacement, and accelerometers were measured. With a good data acquisition capability of a camera, the need to develop a unified image and video analysis application was investigated by Luo et al. [14]. A new technique, InnoVision, a video image processing technique, was developed to address challenges associated with vision sensors for SHM. The three critical difficulties, limited lighting, multi-point displacement, and camera vibration in the field associated with vision sensors, were addressed. Moreover, the digital cameras, the plenty of recent low-cost and high-description video cameras found their use in various Structural Health Monitoring applications where the video camera was utilized as a piece of remote monitoring equipment. The MM technique by Chen et al. [15] utilized high-speed to visualize and quantify the mode shapes of structures. In a subsequent study, Chen et al. [16] presented a video camera-based vibration

measurement study as a proof-of-study in which an antenna tower on top of a building was measured from over 175 m. The use of noncontact techniques also offers an encouraging way for modal identification. Feng and Feng [17] aimed to link displacement mea-surement with the vision method by simultaneous identification of structural stiffness and excitation forces. The robust subpixel OCM algorithm was applied to track the structural displacement of the bridge. The problem correlated with the use of cameras during different weather conditions was appraised by Kim et al. [18] using various image processing techniques. The results showed only a 1% variation in camera-based measurement with respect to accelerometers. As presented above, the use of video cameras and the related image processing algorithms form a large diversity of noncontact methods for different Structural Health Monitoring applications. Although the recent use of vision-based sensors in numerous applications of Structural Health Monitoring, there are several challenges that are currently affecting the efficiencies of vision-based methods. Factors including weather conditions such as wind, rain, light, snow, fog, and the surrounding vibrations as well as the accuracy of camera-based measurements under small-amplitude motion need to be explored in the context of SHM.

In this paper, to overcome some of the limitations of previous vision-based methods such as an expensive speed camera, the low contrast and effect of haze on the captured images and obtain higher quality results from the captured images with more contrast, an image processing methodology is proposed using shiny targets with an economy camera. First, the method of matching and scaling recorded videos is described. Then, the theory of extracting natural frequencies of a structure due to the ambient vibration in the time domain is briefly stated. Then, as a field test, the geometry and characteristics of the Tabiat bridge are described. Afterward, extracted frequencies of the bridge from the seismic sensors and the proposed method are compared together.

2. Proposed Vision Sensor System

Vision-based displacement sensors provide a simple, cost-effective, and precise alternative for far displacement monitoring. Numerous vision-based displacement sensor systems are enabled by the template matching techniques, with pattern matching [19], edge detection, digital image correlation (DIC) [20], Hough transforms [21], the RANSAC algorithm [22], the optical flow-based method [23], the up sampled cross-correlation (UCC) and orientation code matching (OCM) [24], etc.

Recently, efforts have also been made to investigate the feasibilities of displacement measurements utilizing the advanced onboard sensing capabilities of the software technologies, such as embedded high-resolution/speed video features, powerful fast computers, open-source computer vision libraries, etc.

Nonetheless, most of the existing vision-based sensors have one or more of the following restrictions in practical applications: (1) The approved template matching techniques give motion with integer-pixel resolution since the minimum unit in a video image is one pixel. Though in many applications, the pixel-level precision is acceptable, it is often far from the required precision in case of small structural vibrations; (2) Most current vision sensor systems can only be used for post-processing the recorded data. They thus cannot execute real-time displacement measurement, which limits their application for online monitoring; (3) It is evident that the precision of the template matching methods relies mainly on the image quality, which is often difficult to guarantee in outdoor field conditions such as brightness variation, partial target obstruction, partial shading, background disorderliness, etc.

2.1. Template Matching and Scaling Factor Determination

The vision sensor system simply consists of a video camera and a notebook laptop. In the performance, an area in the image of a sequence of frames captured is selected as a template. The template will be located in consecutive images using template matching techniques. Therefore, the displacements are recorded in pixels that can be subsequently transformed into physical displacement in millimeters via a scaling factor. To develop measurement accuracy, subpixel registrations must be incorporated into the template

matching algorithm. In this study, based on the OCM template matching algorithm and subpixel bilinear interpolation, the software is developed to accurately track structural displacements at user-defined locations frame-by-frame (Figure 1). Also, more details about OCM principle are in [19]. Then, to record structural displacements from the video camera, the establishment of the relationship between the pixel coordinate and the physical coordinate is demanded. The scaling factor (e.g., with units of mm/ pixel) can be collected in two ways: First, it is calculated from the known physical dimension on the object surface and its analogous image dimension in pixels; Second, it is calculated by intrinsic parameters of the camera as well as the extrinsic parameters between the camera and the object structure. The first method scaling factor is selected in this study.

After target registration, any texture on the structural surface can be registered as a tracking target, as long as it has pattern contrast compared with the surrounding background, e.g., existing surface features such as bolt/rivet connection, but installing targets on structures and capturing images from close distances have some limitations, such as the need to install the camera in a fixed place outside the monitored structure, and it is almost impossible to take pictures from a close distance in many structures such as bridges. Therefore, it is necessary to use expensive high-speed cameras to capture images with good quality for image processing and extract structural displacements. This issue can make the image processing method uneconomical [16]. Therefore, to overcome this limitation, this study suggests installing bright targets on the structural elements and recording the video with an economical camera from a long distance to extract the structure's displacements. These bright targets help provide high-quality images with higher contrast for image processing. For capturing images with higher contrast, it is more appropriate to use bright targets with concentrated light, such as LEDs, which, if taken at night, will reduce the image clarity and contrast of the bright target and, as a result, the quality of the captured images. It will be higher. However, it should be noted that the proposed method does not eliminate other limitations in image processing methods, such as the camera base vibration.

In this study, to observe and record a better image by better quality, a target with a good shine such as LED has selected. Then template matching operated for displacement, the amount of time it takes depends on the target searched within the whole frame or part image of each video recorded frame. To reduce the calculation time, the searching area could be limited to a predefined region of interest (ROI) near the template's Pattern.

3. Stochastic Subspace Identification (SSI) Method

3.1. State-Space Model

The dynamic behavior of a structure is usually represented in the time domain as:

$$\boldsymbol{M}\ddot{U}(t)+\boldsymbol{C}\dot{U}(t)+\boldsymbol{K}U(t)=F(t) \tag{1}$$

where $\ddot{U}(t)$, $\boldsymbol{C}\dot{U}(t)$ and $U(t)$ are the vectors of acceleration, velocity, and displacement,

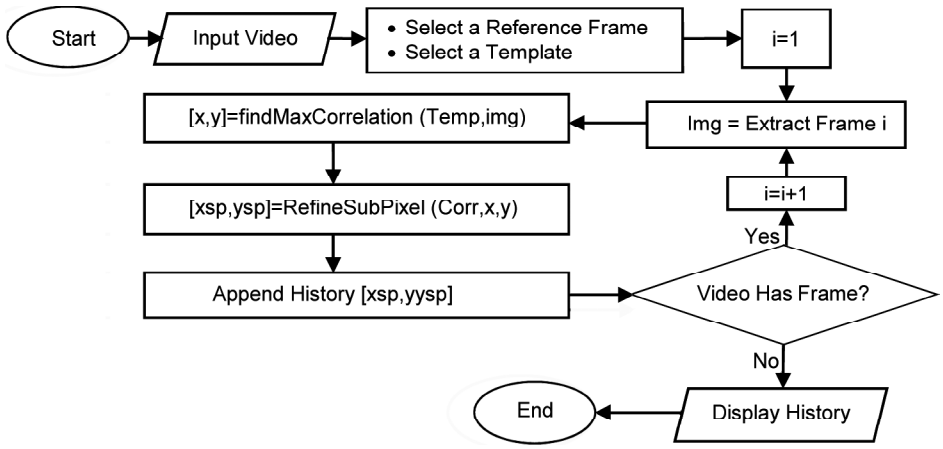

Figure 1. Flowchart of vision sensor based on OCM.

respectively; $\boldsymbol{M}$, $\boldsymbol{C}$, and $\boldsymbol{K}$ denote the mass, damping, and stiffness matrices, respectively and $F(t)$ is the force vector. The above second-order differential equation can be converted to the first-order differential equation using state space representation:

$$\dot{\boldsymbol{x}}(t) = \boldsymbol{A}_c \boldsymbol{x}(t) + \boldsymbol{B}_c \boldsymbol{u}(t) \tag{2}$$

where $\boldsymbol{x}(t) = [U(t), \dot{U}(t)]^T$ is the state vector; $\boldsymbol{A}_c$ and $\boldsymbol{B}_c$ are respectively the state matrix and input matrix:

$$\boldsymbol{A}_c = \begin{bmatrix} 0 & \boldsymbol{I}_n \\ -\boldsymbol{M}^{-1}\boldsymbol{K} & -\boldsymbol{M}^{-1}\boldsymbol{C}_2 \end{bmatrix}, \quad \boldsymbol{B}_c = \begin{bmatrix} 0 \\ \boldsymbol{M}^{-1}\boldsymbol{B}_2 \end{bmatrix} \tag{3}$$

where $\boldsymbol{I}_n$ is the unit matrix and n is the number of degrees of freedom of the structure.

The response of a dynamic structure is usually quantified by accelerometers, velocimeters and displacement meters, and therefore the observation equation can be written as:

$$y(t) = \boldsymbol{C}_a \ddot{U}(t) + \boldsymbol{C}_v \dot{U}(t) + \boldsymbol{C}_d U(t) \tag{4}$$

substituting the state vector, Equation (4) can be rewritten as:

$$y(t) = \boldsymbol{C}_c x(t) + \boldsymbol{D}_c u(t) \tag{5}$$

Equations (2) and (5) develop the state-space presentation of the dynamic structure in a continuous-time form. In practice, the response data are always recorded in a discrete form, so the continuous-time model must be transformed to the corresponding discrete format:

$$\begin{cases} x_{k+1} = \boldsymbol{A}x_k + \boldsymbol{B}u_k \\ y_k = \boldsymbol{C}x_k + \boldsymbol{D}u_k \end{cases} \tag{6}$$

where $\boldsymbol{x}_k = \boldsymbol{x}(k\Delta t)$ is a discrete time state vector; $\boldsymbol{A} = exp(A_c \Delta t)$ is a discrete state matrix; $\boldsymbol{B}$ is a discrete input matrix.

It should be emphasized that it is unavoidable for the response signal to be contaminated with random (noise) components. Commonly, such uncertainty components are divided into process noise w_k and measurement noise v_k. Thus, Equation (6) can be expressed as the following discrete state space model:

$$\begin{cases} x_{k+1} = \boldsymbol{A}x_k + \boldsymbol{B}u_k + \boldsymbol{w}_k \\ y_k = \boldsymbol{C}x_k + \boldsymbol{D}u_k + \boldsymbol{v}_k \end{cases} \tag{7}$$

Assuming that the excitation acting on the dynamic structure can be behaved as a white noise process, the last two items on the right-hand side of Equation (7) can be merged:

$$\begin{cases} x_{k+1} = \boldsymbol{A}x_k + \boldsymbol{w}_k \\ y_k = \boldsymbol{C}x_k + \boldsymbol{v}_k \end{cases} \tag{8}$$

In Equation (8), the stochastic terms of both $\boldsymbol{w}_k$ and $\boldsymbol{v}_k$ are assumed to be a zero-mean white noise process with covariance matrices as

$$E\left(\begin{bmatrix} \boldsymbol{w}_k \\ \boldsymbol{v}_p \end{bmatrix} \begin{bmatrix} \boldsymbol{w}_p^T & \boldsymbol{v}_q^T \end{bmatrix}\right) = \begin{bmatrix} Q & S \\ S^T & R \end{bmatrix} \delta_{pq} \tag{9}$$

3.2. Identification of the System Matrices

The Hankel matrix is defined as:

$$Y_{0|2i-1} = \frac{1}{\sqrt{j}} \begin{bmatrix} y_0 & y_1 & \cdots & y_j \\ \vdots & \vdots & \ddots & \vdots \\ y_{i-2} & y_{i-1} & \cdots & y_{i+j-3} \\ y_{i-1} & y_i & \cdots & y_{i+j-2} \\ \hline y_i & y_{i+1} & \cdots & y_{i+j-1} \\ y_{i+1} & y_{i+2} & \cdots & y_{i+j} \\ \vdots & \vdots & \ddots & \vdots \\ y_{2i-1} & y_{2i} & \cdots & y_{2i+j-2} \end{bmatrix} = \frac{1}{\sqrt{j}} \begin{bmatrix} Y_{0|i-1} \\ \hline Y_{i|2i-1} \end{bmatrix} = \frac{1}{\sqrt{j}} \begin{bmatrix} Y_p \\ \boldsymbol{Y}_f \end{bmatrix} \tag{10}$$

where the Hankel matrix $Y_{0|2i-1}$ consists of "$2i$" block rows and "j" columns. It can be divided into two parts: "the past" Y_p and "the future" Y_f, both of which consist of i block rows. In practice, the Hankel matrix can be established directly based on the response signal from the structure. The so-called block Toeplitz matrix $T_{l/i} \in \boldsymbol{R}^{li \times li}$ can be divided:

$$T_{l|i} = \boldsymbol{Y}_f \boldsymbol{Y}_p = \begin{bmatrix} CA^{i-1} & CA^{i-2}G & \ldots & CG \\ CA^{i}G & CA^{i-1}G & \ldots & CAG \\ \vdots & \vdots & \ddots & \vdots \\ CA^{2i-2}G & CA^{2i-3}G & \ldots & CA^{i-1}G \end{bmatrix} = \begin{bmatrix} C \\ CA \\ \vdots \\ CA^{i-1} \end{bmatrix} \begin{bmatrix} A^{i-1} & \ldots & AG & G \end{bmatrix} = \Gamma_i \Delta_i \tag{11}$$

$$\Gamma_i = \begin{bmatrix} C \\ CA \\ \vdots \\ CA^{i-1} \end{bmatrix}, \quad \Delta_i = \begin{bmatrix} \boldsymbol{A}^{i-1} & \dots & \boldsymbol{AG} & \boldsymbol{G} \end{bmatrix} \quad (12)$$

where, Γ_i, Δ_i are the extended observable matrix and the inversely extended controllable matrix, respectively.

Through SVD manipulation, the Toeplitz matrix can be broken down as:

$$T_{1|i} = \mathrm{US}V^T = \begin{bmatrix} \boldsymbol{U}_1 & \boldsymbol{U}_2 \end{bmatrix} \begin{bmatrix} \boldsymbol{S}_1 & 0 \\ 0 & 0 \end{bmatrix} \begin{bmatrix} \boldsymbol{V}_1^T \\ \boldsymbol{V}_2^T \end{bmatrix} = U_1 S_1 V_1^T = \left(\boldsymbol{U}_1 \boldsymbol{S}_1^{1/2} \boldsymbol{T}\right)\left(\boldsymbol{T}^{-1} \boldsymbol{S}_1^{1/2} \boldsymbol{V}_1^T\right) \quad (13)$$

where $\boldsymbol{U}$ and $\boldsymbol{V}$ are orthogonal matrices, and T is a non-singular matrix. One can use the unit matrix I instead of T in practice.

Replacing T with I in Equation (13), and contrasting this equation with Equation (11)

$$\Gamma_i = U_1 \boldsymbol{S}_1^{1/2}$$
$$\boldsymbol{\Delta_i} = \boldsymbol{S}_1^{1/2} \boldsymbol{V}_1^T \quad (14)$$

According to Equations (13) and (14), $T_{2/i+1}$ can be concluded:

$$T_{2|i+1} = \Gamma_i \mathrm{A} \Delta_i^d = \begin{bmatrix} CA^i G & CA^{i-1}G & \dots & CAG \\ CA^{i+1}G & CA^i G & \dots & CA^2 G \\ \vdots & \vdots & \ddots & \vdots \\ CA^{2i-1}G & CA^{2i-2}G & \dots & CA^i G \end{bmatrix} \quad (15)$$

It is clear that $T_{2/i+1}$ can be calculated directly based on the output records. Substituting Equation (14) into the Equation (15), we have

$$A = \boldsymbol{S}_1^{-1/2} \boldsymbol{U}_1^T T_{2/i+1} V_1 \boldsymbol{S}_1^{-1/2} \quad (16)$$

From Equation (12), the matrix C is a sub-matrix, or the first l rows of T_i; while the matrix G is the last l columns of Δ_i. Therefore, both of the matrix's A and C can be obtained.

4. Field Test: Tabiat Bridge

The vision-sensing techniques are further demonstrated in the field test conducted on the Tabiat Bridge. To verify the vision-based system identification method, wireless seismic sensors have been tested separately. Tabiat Bridge is a famous two-level pedestrian steel truss bridge with a 270 m long span and 28 m height. The structural system consisting of more than 6,000 truss elements and joints, opened in 2013. Tabiat bridge is one of the main attractions of Tehran located above a high-way with heavy traffic in the city. Also, it has access to lots of people every day as well as pedestrians and athletes, and customers of restaurants and coffee shops located on the first level of the bridge. Therefore, it is a good field structure that experiences very good ambient vibration.

4.1. Seismic Sensor Data Acquisition

In this test, seismic sensors (Lennartz sensors) were used along the bridge, and the results were compared with the vision-based method to verify vision-based method results. Measured data from the sensor which has been installed at the mid-span of the bridge were used as a common node to use its results for obtaining mode shapes from different field data recording. To conduct the ambient vibration tests, four tri-axial seismic sensors, LE-3D/20s from Lennartz Company, are utilized. With these four sensors and selecting 1 common node (node 1344 in Figure 2), 19 joints along the bridge due to the ambient vibration were recorded. Because each joint essentially acts as a multi-degree-of-freedom (MDOF) system, the ambient seismic data recorded by the LE-3D/20s would be adequate for capturing the fundamental natural periods of the system. The sensor has three velocity recording channels in three orthogonal cartesian directions. The sensor is connected to a data logger that records the velocity data (Figure 3). This sensor has three input channels with 24-bit ADC resolution. The technical details of the instrumentation are listed in Table (1).

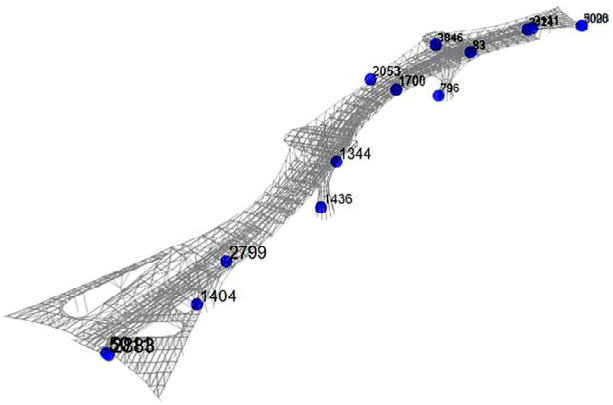

Figure 2. Seismic Sensors location on the access way and orientation from the bridge's 3D view.

Figure 3. Seismic sensor along with the data logger and other accessories.

Table 1. Technical specification of sensor.

Lennartz Model	LE-3D/20s
Sensitivity	1000 V/m/s
Natural Frequency	0.05 Hz
Upper Corner Frequency	~50 Hz
Full-Scale Output Voltage	±10 V (Suitable for Differential Operation)
Damping	0.707 critical
Dimensions	195 mm Diameter, 165 mm Height
Weight (not Including Transport Box)	6 kg
Temperature Rang	-15 ... +65 °C
Supply Current@12V DC	50 mA (Idle) ... 100 mA (Peak Amplitude)
Warm-Up Time	2 Minutes

4.2. Vision-Based Method Data Acquisition

To record data by vision-based method, the target such as a red-light LED was installed on a component, and data was recorded, so the bridge responses are reflected by the measured rotations. The economy video camera was located in the location under the bridge at around 39 m away from the target in mid span of the Tabiat Bridge to capture and record vibrational responses. Based on a wired sensor study, the first six main frequencies of the Target Bridge are under 3 Hz. The displacement sampling rate in this field experiment was set to 3 Hz, which is sufficient for this study as well as future analyses of higher-order modes.

Sensors along the bridge near the joints on the access way as shown in Figure (4). The LED point was also contracted and stabilized on each member as shown in Figure (5) and the ambient vibration of the bridge was mainly because of passing traffic through the adjacent highway as well as pedestrian

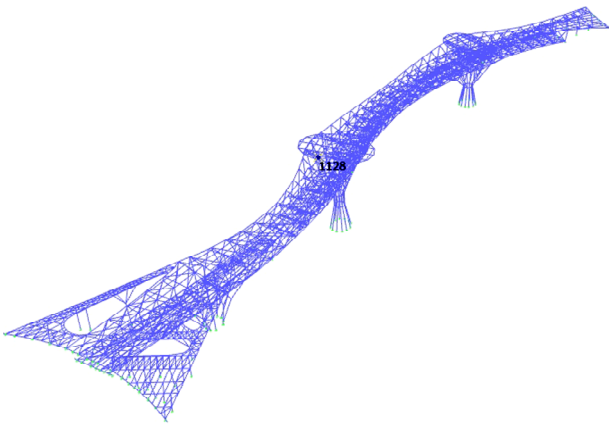

Figure 4. Vision-based sensors location on the access way and orientation from the bridge's 3D view.

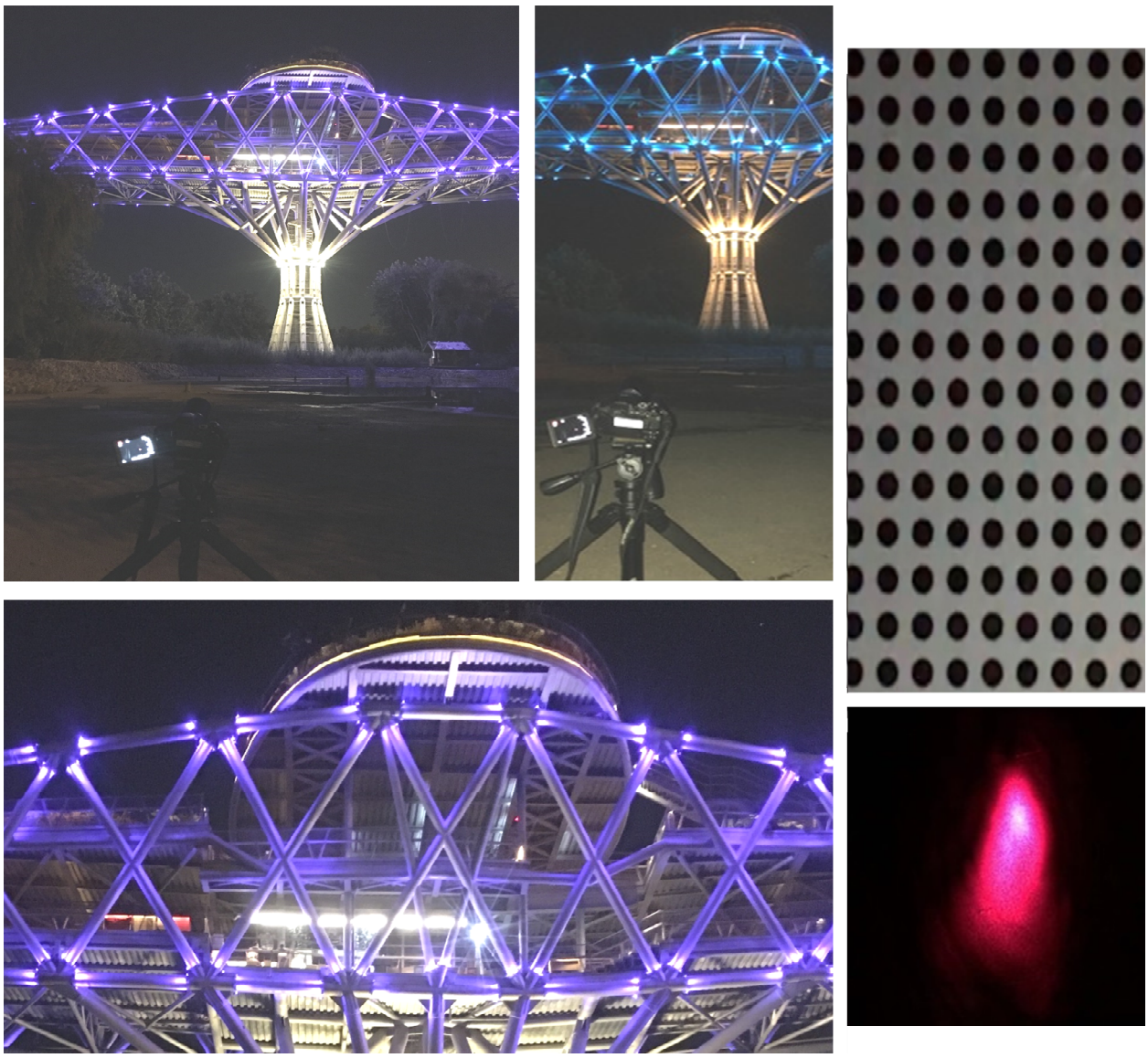

Figure 5. Vision-based Sensor setup from the bridge's 3D view.

Table 2. LED technical specifications.

Semiconductor Material	Wavelength	Color	VF@20mA
GaAsP	630-660 nm	Red	1.8v

Table 3. Camera technical specifications.

Model	Lens	Image Sensor	Vibration Reduction
Nikon, COOLPIX B700	NIKKOR Lens with 60 x Optical Zoom	1/2.3-in. Type CMOS	Lens-Shift VR

movement on the bridge. The air temperature was around 27°C.

In following, in the vision-based method, the LED was installed on an element of the structure of the Tabiat Bridge. The LED target was obtained by video camera tracking. The economy video camera (Nikon, COOLPIX B700) with CMOS-type sensor and 1280×720 pixels selected as a 240 FPS frame rate. The LED and camera technical specifications have shown in Tables (2) and (3), respectively.

4.3. Results of the Ambient Vibration Test

The ambient velocity of the Tabiat bridge joints in three-orthogonal axes was recorded continuously for 30 minutes, with a rate of 200 samples per second. Data was recorded in two orthogonal lateral directions as well as vertical directions. Parts of the reference sensor recorded data in the three different directions are shown in Figure (6). The velocity intensity reaches 0.5-1 mm/s in directions.

Due to the ambient excitation, the recorded data contains the main dynamic properties of the bridge. Considering the expected frequency range of the bridge (0.5-10 Hz) the noise and its elimination could be important. For this purpose, examining the data and applying their frequency content before and after the filter application has been studied.

As shown in Figure (7), the time history diagram before and after the noise filtration has no specific effect on the output results and their Fast Fourier Transform (FFT) before and after the filter is almost the same in the desired frequency range. Figure (8) shows the displacement time history of LED that is extracted from the vision-based method in two different directions. Also, the Fast Fourier Transform of extracted time histories is shown in Figure (8).

4.3.1. Data Analyzed by Stochastic Subspace Identification (SSI)

In the previous section, the mathematical theory

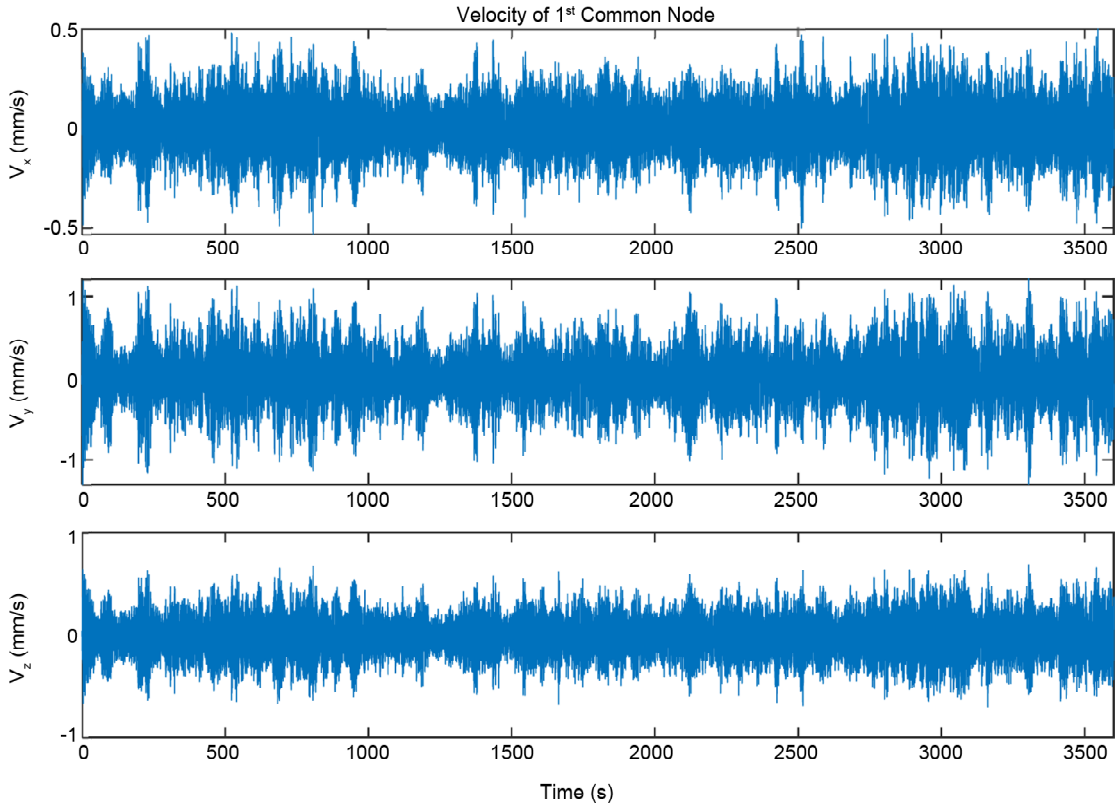

Figure 6. Seismic Sensor Time history of data for the common node.

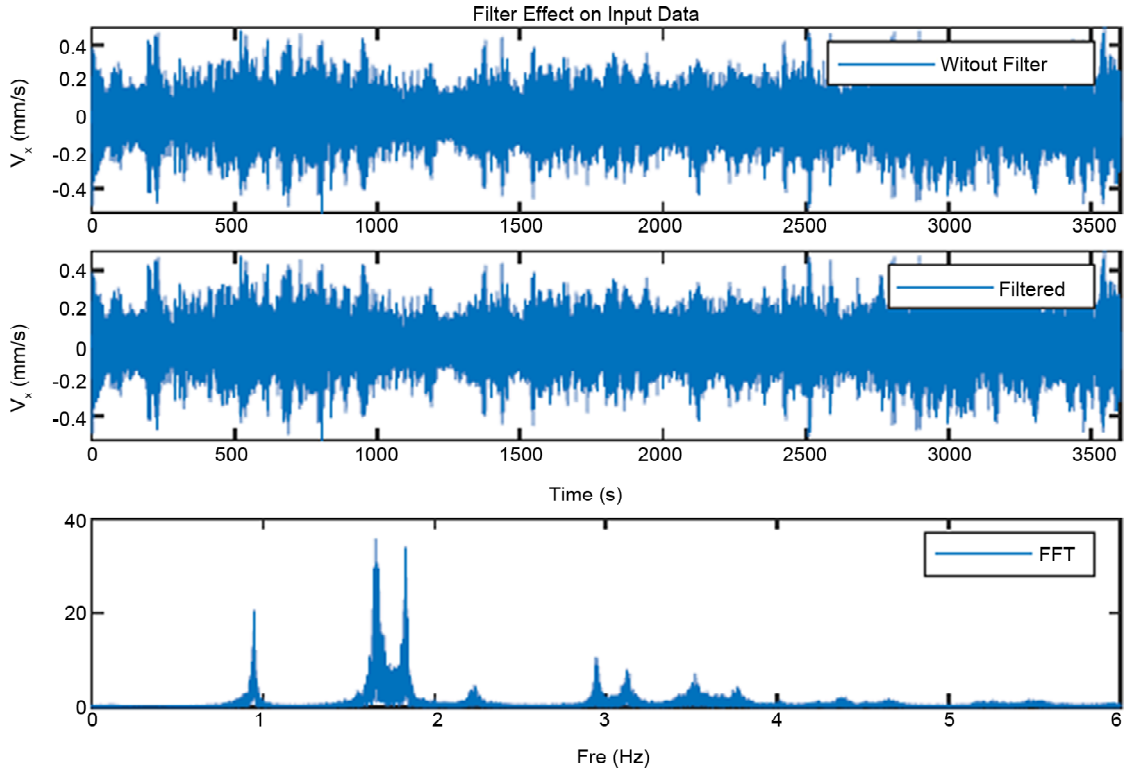

Figure 7. Time history diagram of seismic sensor data in the reference node before the filter, after the filter and with Fourier Transform.

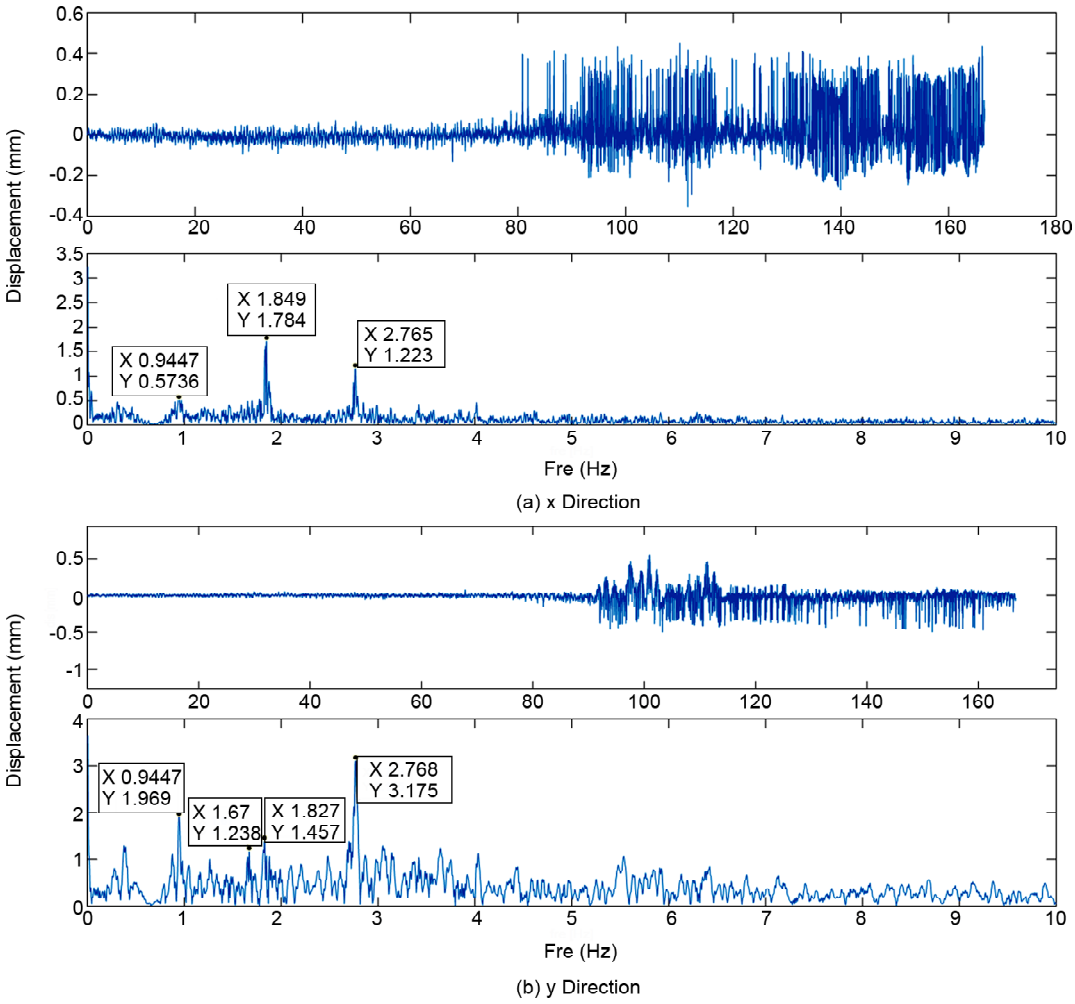

Figure 8. Time history diagram of Vision-based data.

of stochastic subspace identification was studied briefly [13, 25]. This method needs less inputting information and it can extract dynamic characteristics for multiple modes together [26]. Also, this method has some restrictions. For example, when using a subspace recognition path to extract dynamic characteristics, the system sequence of the identification model must be selected. When there are large amounts of data, the SSI algorithm needs more memory and calculation time [27]. Thus, the SSI method has been used to obtain the natural frequencies of the bridge for both recorded data from the seismic sensors and vision-based sensors. Figures (9) and (10) shows SSI diagram for the seismic sensors data and vision-based sensors, respectively. The obtained results from different

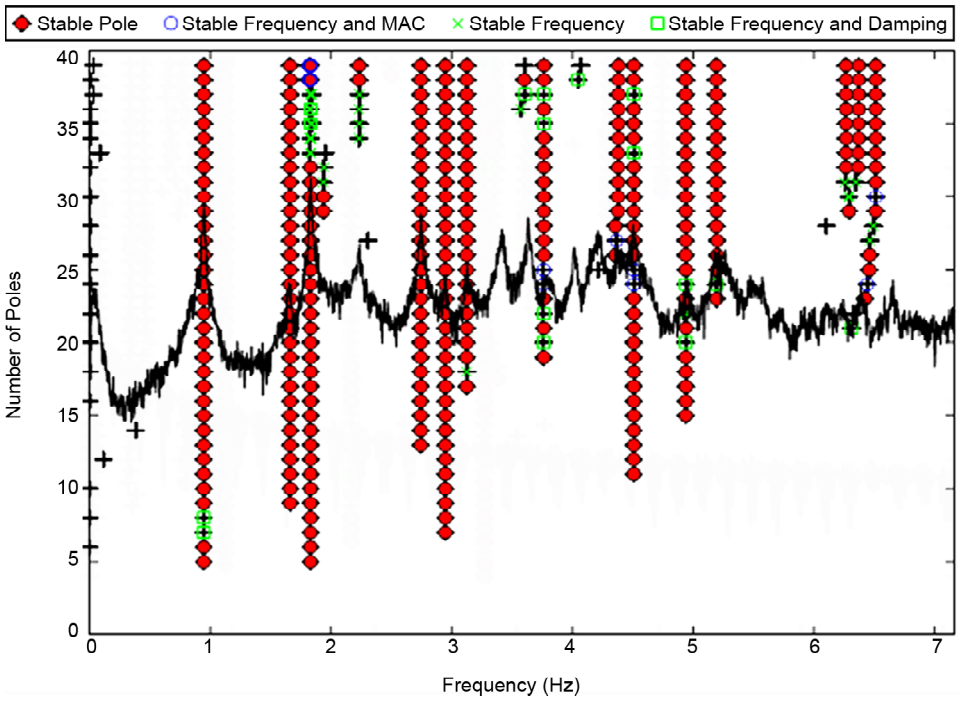

Figure 9. Seismic sensors data stability diagram of seismic sensor.

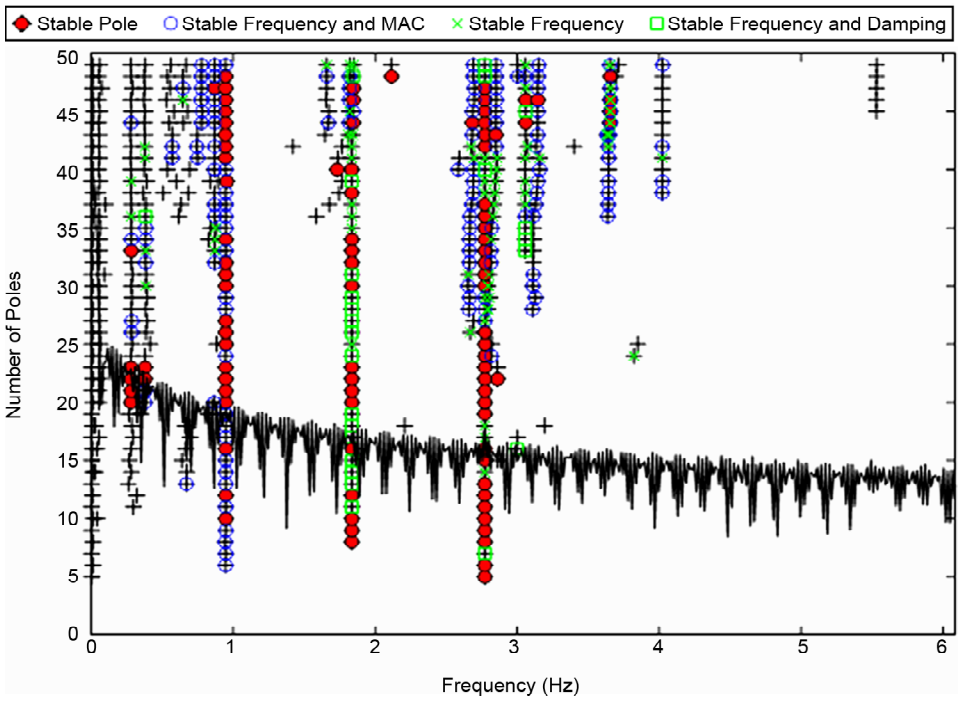

Figure 10. Data stability diagram of vsion base sensor.

methods are compared in Table (4) and Figure (11). The results show that the proposed technique can estimate five natural frequencies of the bridge with very good accuracy without using any high-quality and expensive sensors.

Figure (12a) shows the motion of the bolt on one of the connections of the bridge in two orthogonal directions and their Fast Fourier Transforms (FFT) that are extracted from captured videos with an economical camera. To observe the capability of a shiny target. This test has been done under similar conditions such as distance of the camera to the structure, video recording condition, etc.

As shown in Figure (12b), SSI diagram of the extracted bolt motions does not give any clear frequencies for the structure while using shiny target shows acceptable dynamic characteristics results.

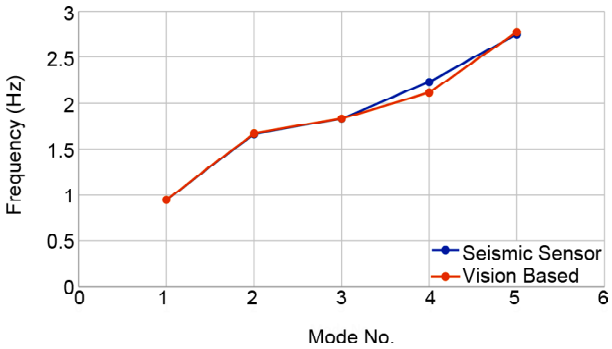

Figure 11. Natural frequencies extracted from seismic sensors and vision-based method.

Table 4. Comparison of structure main frequencies.

Mode No.	Lenartz Sensor	Vision Based Sensor
First	0.946	0.945
Second	1.664	1.671
Third	1.833	1.835
Forth	2.232	2.115
Fifth	2.748	2.772

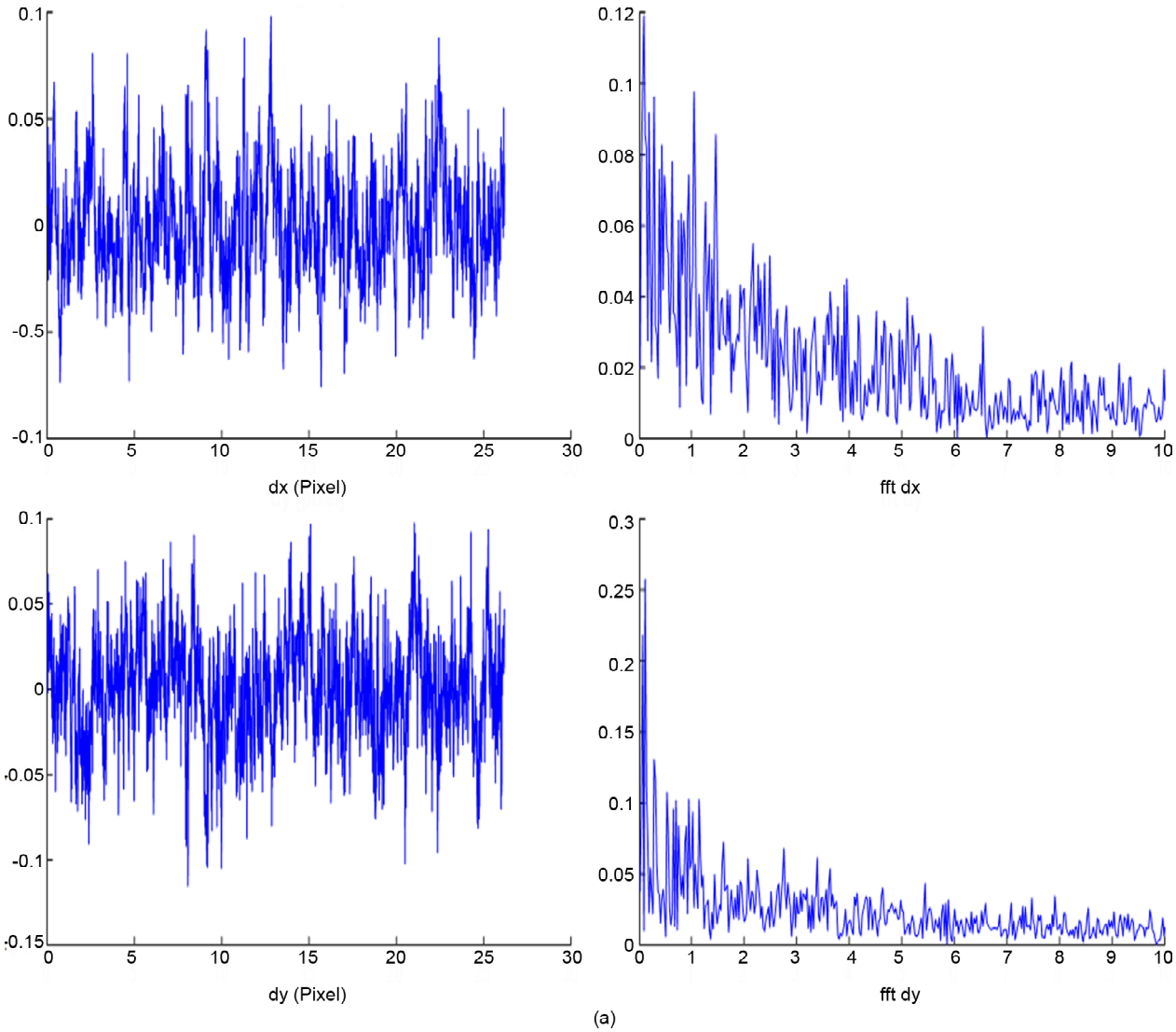

Figure 12. The data acquisition results do not extract the frequencies responses.

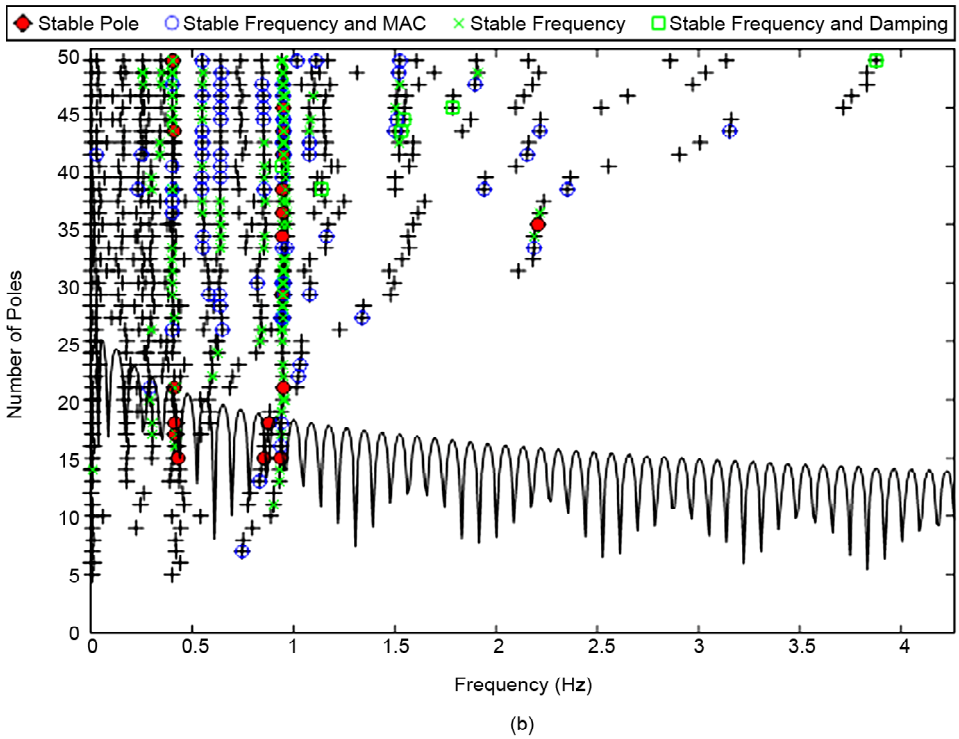

(b)

Figure 12. Continue.

5. Conclusion

In this paper, a new technique has been proposed for vision-based system identification using shiny targets. In this technique, a LED is attached to one of the main elements of the structure that experience significant vibrations due to the ambient loading. Then, the motion of the LED target is captured by an economy camera and converted to displacement using template matching and scaling factor techniques. A truss steel bridge is used as a field study for which dynamic frequencies are obtained using seismic sensors and vision-based methods. The proposed system identification method could detect the first five frequencies of the bridge in good agreement with those obtained from the seismic sensors data. The present study results show that using shiny targets helps to identify structural displacements more clearly. Thus, dynamic characteristics of structure could be extracted more accurately. In other words, system identification through displacement measurement using the proposed vision-based method can provide more accurate gauge-free measurements of the dynamic displacements for various types of structures through simple installations and economy cameras.

References

1. Beskhyroun, S., Wegner, L.D., Sparling, B.F. (2011) New methodology for the application of vibration-based damage detection techniques. *Struct Control Health Monit*, **19**(1), 88-106.

2. Knecht, A. and Manetti, L. (2001) Using GPS in structural health monitoring. *Smart Structures and Materials 2001: Sensory Phenomena and Measurement Instrumentation for Smart Structures and Materials*, 4328: 122-129.

3. Yi, T.H., Li, H.N., and Gu, M. (2010) Recent research and applications of GPS based technology for bridge health monitoring. *Sci China Technol. Sci.*, **53**(10), 2597-2610.

4. Park, H.S., Lee, H.M., Adeli, H., and Lee, I. (2007) A new approach for health monitoring of structures: terrestrial laser scanning. *Comput Aided Civ Inf Eng.*, **22**(1), 19-30, SONY ET AL. 17 of 22.

5. Leong, W.H., Staszewski, W.J., Lee, B.C., Scarpa, F. (2005) Structural health monitoring using scanning laser vibrometry: III. Lamb waves for fatigue crack detection. *Smart Materials and Structures*, **14**(6), 1387-1395.

6. Gu, C., Rice, J.A., and Li, C. (2012) A wireless smart sensor network based on multi-function interferometric radar sensors for structural health monitoring. *IEEE Topical Conference on Wireless Sensors and Sensor Networks*, 33-36.

7. Pieraccini, M., Fratini, M., Parrini, F., Atzeni, C., and Bartoli, G. (2008) Interferometric radar vs. accelerometer for dynamic monitoring of large structures: an experimental comparison. *NDT and E International*, **41**(4), 258-264.

8. Molina-Viedma, A., Felipe-Sesé, L., Lopez-Alba, E., and Diaz, F. (2018) High-frequency mode-shapes characterisation using digital image correlation and phase-based motion magnification. *Mech Syst Signal Proces*, **102**, 245-261.

9. Trebuna, F. and Hagara, M. (2014) Experimental modal analysis performed by high-speed digital image correlation system. *Measurement*, **50**, 78-85.

10. Feng, M.Q., Fukuda, Y., Feng, D., and Mizuta, M. (2015) Nontarget vision sensor for remote measurement of bridge dynamic response. *J. Bridge Eng.*, **20**(12), 4015023.

11. Walker, K. (2015) Use of virtual visual sensors in the determination of natural frequencies of timber structures for structural health monitoring. In: *Master of Science Thesis*. Oregon State University.

12. Fukuda, Y., Feng, M.Q., and Shinozuka, M. (2010) Cost-effective vision-based system for monitoring dynamic response of civil engineering structures. *Struct Control Health Monit.*, **17**(8), 918-936.

13. Feng, D. and Feng, M.Q. (2015) Vision-based multipoint displacement measurement for structural health monitoring. *Struct Control Health Monit.*, **23**(5), 876-890.

14. Luo, L., Feng, M.Q., and Wu, Z.Y. (2018) Robust vision sensor for multi-point displacement monitoring of bridges in the field. *Eng Struct.*, **163**, 255-266.

15. Chen, J.G., Wadhwa, N., Cha, Y.J., Durand, F., Freeman, W.T., and Buyukozturk, O. (2015) Modal identification of simple structures with high-speed video using motion magnification. *J. Sound Vibration*, **345**, 58-71.

16. Chen, J.G., Davis, A., Wadhwa, N., Durand, F., Freeman, W.T., and Büyükoztürk, O. (2014) Video camera - based vibration measurement for civil infrastructure applications. *J. Infrast Syste.*, **23**, 1-11.

17. Feng, D. and Feng, M.Q. (2017) Identification of structural stiffness and excitation forces in time domain using noncontact vision-based displacement measurement. *J. Sound Vibration*, **406**, 15-28.

18. Kim, S.W., Jeon, B.G., Cheung, J.H., Kim, S.D., and Park, J.B. (2017) Stay cable tension estimation using a vision-based monitoring system under various weather conditions. *J. Civil Struct Health Monit.*, **7**(3), 343-357.

19. Ye, X.W., Ni, Y.Q., Wai, T.T., Wong, K.Y., Zhang, X.M., and Xu, F. (2013) A vision-based system for dynamic displacement measurement of long-span bridges: algorithm and verification, *Smart Struct. Syst.*, **12**(2013), 363-379.

20. Busca, G., Cigada, A., Mazzoleni, P., and Zappa, E. (2014) Vibration monitoring of multiple bridge points by means of a unique vision-based measuring system, *Exp. Mech.*, **54**, 255-271.

21. Song, Y.-Z., Bowen, C.R., Kim, A.H., Nassehi, A., Padget, J., and Gathercole, N. (2014) Virtual visual sensors and their application in structural health monitoring, *Struct. Health Monit.,* **13**, 251-264.

22. Ribeiro, D., Calçada, R., Ferreira, J., and Martins, T. (2014) Non-contact measurement of the dynamic displacement of railway bridges using an advanced video-based system, *Eng. Struct.*, **75**, 164-180.

23. Caetano, E., Silva, S., and Bateira, J. (2011) A vision system for vibration monitoring of civil engineering structures, *Exp. Tech.*, **35**, 74-82.

24. Feng, D. and Feng, M.Q. (2016). Vision-based multipoint displacement measurement for structural health monitoring. *Structural Control*

and Health Monitoring, **23**(5), 876-890.

25. Ramezani, M. and Bahar, O. (2021) Indirect structure damage identification with the information of the vertical and rotational mode shapes. *Scientia Iranica*, **28**(4), 2101-2118.

26. He, Y.C., Li, Z., Fu, J.Y., Wu, J.R., and Ng, C.T. (2021) Enhancing the performance of stochastic subspace identification method via energy-oriented categorization of modal components. *Engineering Structures*, **233**, 111917.

27. Liu, Y.C., Loh, C.H., and Ni, Y.Q. (2013) Stochastic subspace identification for output-only modal analysis: application to super high-rise tower under abnormal loading condition. *Earthquake Engineering and Structural Dynamics*, **42**(4), 477-498.

28. Chen, G.W., Omenzetter, P., and Beskhyroun, S. (2017) Operational modal analysis of an eleven-span concrete bridge subjected to weak ambient excitations. *Engineering Structures*, **151**, 839-860.